Science of Sintering, **55** (2023)339-351

https://doi.org/10.2298/SOS221014015K

UDK: 681.586; 546.824; 519.718

Humidity Sensing Properties of $(Na_{0.5}Bi_{0.5})_{0.94}Ba_{0.06}$ TiO_3 Lead-Free Ferroelectrics Ceramics

Sadia Kennour[1], Nouara Lamrani[1], Ahcène Chaouchi[1*)], Yannick Lorgouilloux[2], Mohamed Rguiti[2], Christian Courtois[2]

[1]Laboratoire de Chimie Appliquée et Génie Chimique de l'Université Mouloud Mammeri de Tizi-Ouzou, Algérie.

[2]Univ. Polytechnique Hauts-de-France, INSA Hauts-de-France, CERAMATHS-Département Matériaux et Procédés, Valenciennes, F-59313, France.

Abstract:

In this study, the humidity detection properties of the ceramic with composition $(Na_{0.5}Bi_{0.5})_{0.94}Ba_{0.06}TiO_3$, noted (NBT-06BT), were investigated. The NBT-06BT ceramic was synthesized by the semi-solid method and characterized by X-ray diffraction (XRD) and scanning electron microscopy (SEM). The NBT-BT ceramic material sintered at 1100 °C, crystallizes in the tetragonal system without any secondary phase and presents a heterogeneous distribution of polyhedral shaped grains with open intergranular porosities. The electrical and dielectric properties investigations show that the NBT-06BT ceramic material exhibits excellent humidity detection characteristics such as high sensitivity, good linearity and narrow hysteresis. The impedance decreases by three orders of magnitude when the relative humidity increases from 15 % to 90 % at 100 Hz. The maximum hysteresis value of the sensor is 4.69 % RH. The response time and the recovery time are about 68 s and 125 s respectively. Moreover, the sensing mechanism has been discussed in detail by analyzing the complex impedance spectra. These results indicate the potential application of the ceramic material NBT-06BT as a humidity sensor.

Keywords*: Humidity sensor; Lead-free ceramics; Properties; Complex impedance plots; Semi-solid synthesis.*

1. Introduction

Humidity sensors have received considerable attention due to their many applications in industry, agriculture, aeronautics, medicine and meteorology [1-5]. A lot of research has been conducted to develop humidity sensors. In recent years, more and more researchers have been interested in synthesizing new materials for the manufacture of humidity sensors with excellent humidity sensing properties, including high sensitivity, fast response speed, good reproducibility, wide operating range and low cost [6-10].

Ceramic and polymer materials are commonly used as sensing materials for the fabrication of humidity sensors. Ceramic materials based on various metal oxides offer several advantages over polymer materials, such as high chemical and mechanical stability, high reactivity, fast response and a wide operating range [11-17]. Perovskite-type metal oxides[7, 18, 19], have been widely used as dielectrics, ferroelectrics, piezoelectrics, semiconductors and high-temperature ion conductors and have also been considered

*) **Corresponding author:** ahcene.chaouchi@ummto.dz

promising candidates for the manufacture of humidity sensing materials because of their response to humidity over a wide range of operating temperature.

Lead (Pb)-based ceramics such as $PbTiO_3$, $Ca_xPb_{1-x}TiO_3$, Li-$Ca_{0.3}Pb_{0.65}TiO_3$ have been used as humidity sensors in many studies [20, 21], but despite their advantageous dielectric and ferroelectric properties, these Pb-based compounds are toxic and hazardous to human health. Furthermore, waste products from the elaboration and machining of electronic components of various devices cause significant pollution; in particular, lead-based materials are not easily recyclable [22, 23]. For these reasons, research has focused on environmentally friendly lead-free perovskite-based materials with electrical properties comparable to those of lead-based materials. The most commonly used materials for humidity detection are metal oxides such as tin oxide (SnO_2) [17], titanium oxide (TiO_2) [16], zinc oxide (ZnO) [11], cerium oxide (CeO_2) [12], barium titanate ($BaTiO_3$) [13], aluminum oxide (Al_2O_3) [14].

Perovskite-type ABO_3 oxides, in which A are rare earth, alkali and alkaline earth metal ions and B are transition metal ions [9, 24, 25], have been recognized as promising materials for humidity sensing due to their good chemical and thermal stability [4, 26, 13]. Substitution with suitable metal ions in ABO_3 perovskite-type oxides can improve the humidity sensing properties [7, 27]. $(Na_{0.5}Bi_{0.5})_{(1-x)}Ba_xTiO_3$, as an ABO_3-type complex metal oxide with ion substitution at the A site, has been studied by many researchers. Its electrical properties can be tuned by varying the x value [28]. According to previous work [29, 30], there is a low dielectric loss for $(Na_{0.5}Bi_{0.5})_{(1-x)}Ba_xTiO_3$ when x = 0.06 and materials with low dielectric loss and high permittivity may be used to fabricate humidity sensors with good insulating properties and reliability [31].

In this paper, the humidity sensing properties of ceramic $(Na_{0.5}Ti_{0.5})_{0.94}Bi_{0.06}TiO_3$noted (NBT-06BT) were investigated. The crystalline structure and morphology of the NBT-06BT ceramic were characterized by X-ray diffraction (XRD) and scanning electron microscopy (SEM). Humidity sensing properties were obtained by measuring the impedance of the NBT-06BT humidity sensor at different frequencies and different relative humidity levels (RH).

2. Materials and Experimental Procedures

2.1 Preparation of the nanomaterial $(Na_{0.5}Bi_{0.5})_{0.94}Ba_{0.06}TiO_3$

The powder of composition $(Na_{05}Bi_{0.5})_{0.94}Ba_{0.06}TiO_3$ was synthesized by a semi-solid route [32]. The used precursors are: barium nitrate ($Ba(NO_3)_2$), sodium nitrate ($NaNO_3$), bismuth nitrate ($Bi(NO_3)$, $5H_2O$), titanium oxide (TiO_2) and citric acid ($C_6H_8O_7$, H_2O). The salts of metal nitrates were accurately weighed according to stoichiometric proportions, for titanium oxide and nitric acid their equivalent masses to the metal ions of nitrates were calculated. Three solutions were prepared: solution N°(1) was obtained by dissolving 0.3748 g of $NaNO_3$in distilled water, solution N°(2) was obtained by dissolving 2.1293 g of $Bi(NO_3)$, $5H_2O$ in distilled water and solution N°(3) was obtained by dissolving 0.1471 g of $Ba(NO_3)_2$ in distilled water. The three previous solutions were mixed, then 0.7496 g of TiO_2 and 1.9719 g of citric acid were added. The resulting mixture was heated to 70-80 °C for two hours with magnetic stirring to remove the water. After two hours a white viscous solution was obtained. The solution obtained was dried at 100 °C for 24 hours in the oven to obtain a xerogel, which was ground in an agate mortar to obtain a powder. The powder was then calcined at 850 °C.

To manufacture the pellets, an organic binder (polyvinyl alcohol, 5 % by volume) was added manually to the calcined powder and the disks (13 mm in diameter, 2 mm thick) were shaped by uni-axial pressing under a load of approximately 30 kN. The green samples were finally sintered in the air in a tubular furnace for two hours at a temperature of 1100 °C, with heating and cooling rates of 150 °C/h.

2.2. Elaboration of the humidity sensor

The NBT-06BT humidity sensor was elaborated from a disc-shaped sintered pellet (Fig. 1). The silver lacquer was first applied to the center of the two flat surfaces of the discs and then the pellets were dried in an oven at 80 °C for 30 minutes. These pellets were then treated at 600 °C for 30 minutes to form the silver electrode. Finally, a copper (Cu) wire was connected to the silver electrodes as a conducting wire.

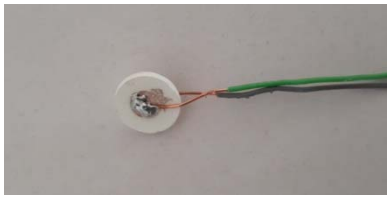

Fig. 1. NBT-06BT humidity sensor.

2.3. Humidity sensor measurement

The humidity sensing properties of the NBT-06BT humidity sensor were measured by a LCR analyzer (HP 4284A). The applied voltage was 1 V a.c. and the frequency varied from 100 Hz to 1 MHz. The NBT-06BT humidity sensor was put inglass-sealed containers with different levels of relative humidity at room temperature to study the humidity sensing property. The glass-sealed containers contained saturated saline solutions (KOH, CH_3COOK, $MgCl_2$, $MgNO_3$, NH_4NO_3, NaCl, KCl and KNO_3) which provided the different RH environments (15 %, 23 %, 34 %, 46 %, 52 %, 72 %, 80 % and 90 %). The container humidity and temperature were also measured using a commercial thermo-hygrometer. The tested humidity sensing material is shown in Fig. 2.

2.4. Characterization

The crystal structure of the NBT-06BT material has been characterized by X-ray diffraction (XRD) using copper X-radiation (Philips X' Pert Pro, Panalytical). The microstructures were observed using a scanning electron microscope (SEM) (Philips XL'30). The electrical properties of the sensor were measured using a HP 4284 meter.

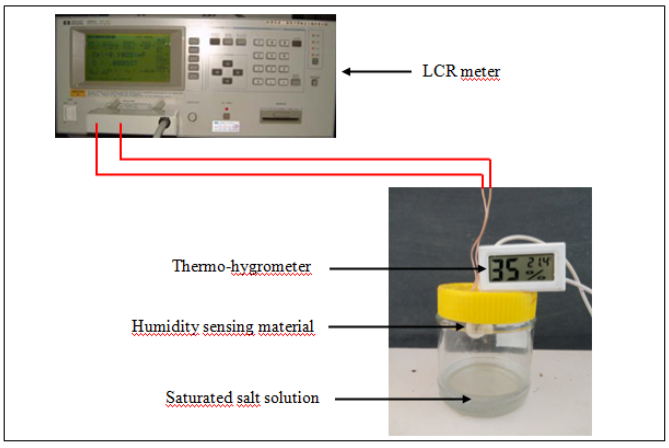

Fig. 2. Tested humidity sensing material.

3. Results and Discussion

3.1. Structural and morphological characterization

The XRD pattern of the NBT-06BT ceramic sintered at 1100 °C for two hours is shown in Fig. 3. The XRD pattern shows intense and fine diffraction peaks indicating good crystallization of the sample in a perovskite structure. No peaks corresponding to a secondary phase have been observed, which shows that the barium (Ba) atom is well diffused in the ($Na_{0,5}$ $Ba_{0,5}$) TiO_3 lattice and forms a solid solution. Indexation of the XRD pattern was performed with the High Score Plus diffraction software and allowed to index the diffraction peaks in the P4mm space group, corresponding to a tetragonal symmetry (JCPDS n°96-210-2069). The obtained cell parameters are a=b=5.5115 A°, c=3.9066 A° and α=β=δ=90°.

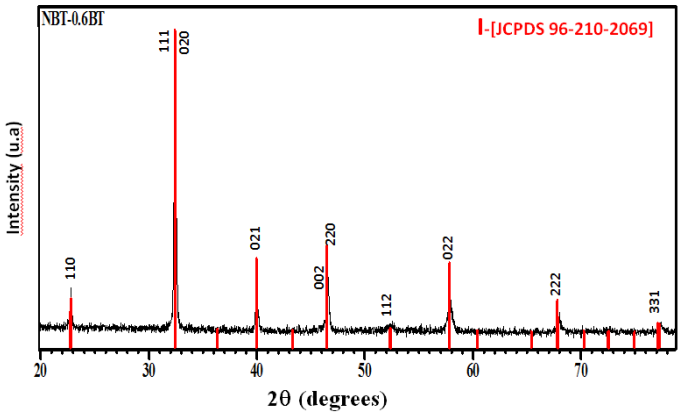

Fig. 3. XRD pattern of NBT-06BT ceramic sintered at 1100 °C/2h.

Fig. 4 shows a SEM micrograph of the NBT-06BT pellet sintered at 1100 °C for 2 hours. The SEM picture shows open intergranular porosities and a distribution of polyhedral shaped grains of heterogeneous size; nanometer-sized grains smaller than 500 nm surround larger grains of sizes between 1 and 3 µm. The presence of porosity is an advantage for the considered application as it increases the water adsorption capacity and therefore it may improve the humidity detection properties of this material.

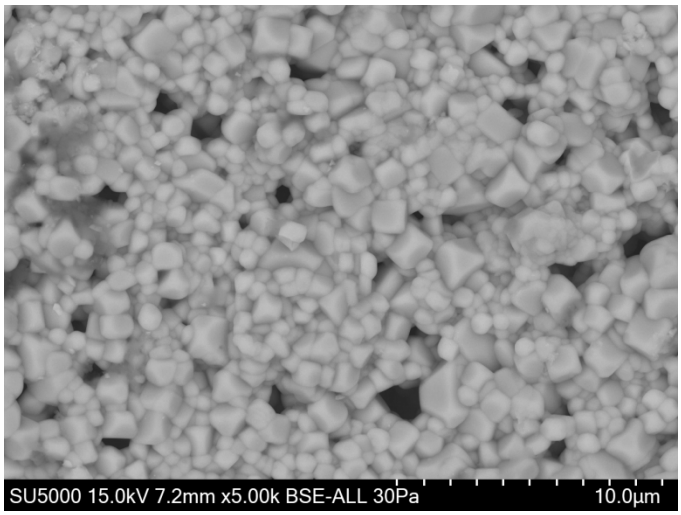

Fig. 4. SEM image of NBT-06BT ceramic sintered at 1100 °C.

3.2. Humidity sensing properties

Fig. 5 shows the curves of capacitance versus relative humidity at different frequencies. From the figure, it can be seen that the capacitance increases with increasing RH at low frequencies, while at high frequencies the capacitance values are low and almost independent of RH.

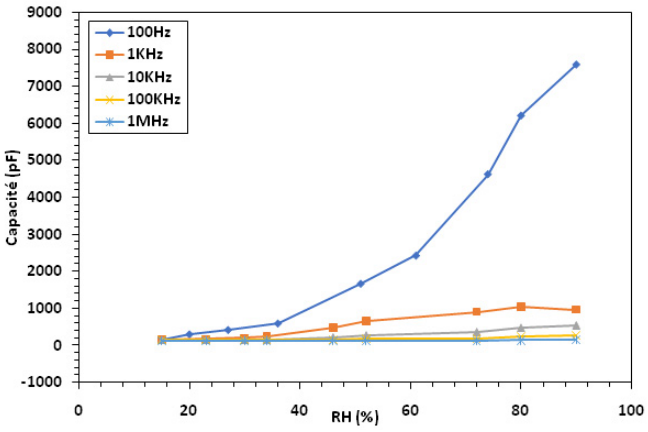

Fig. 5. Capacitance versus RH curves for NBT-06BT humidity sensor at various frequencies.

The variations in capacitance as a function of the frequency of the NBT-06BT sensor at different relative humidity values are shown in Fig. 6. It can be seen that the capacitance value decreases with increasing frequency; a faster decrease is observed at RH = 90 %. The capacitance increases significantly with RH at low frequencies (below 10^4 Hz) while at high frequencies ($f \geq 10^5$ Hz), it is low and independent of humidity.

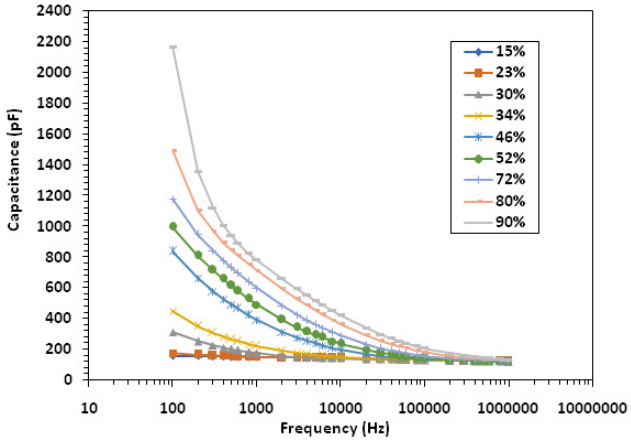

Fig. 6. Capacitance versus frequency curves for NBT-06BT humidity sensor at various relative humidity.

The variation in capacitance is attributed to the polarization capability of the sensing layer in the presence of water molecules. At low relative humidity, only a small amount of water molecules is adsorbed on the sensing layer and water molecules can hardly be polarized. Thus, the NBT-06BT ceramic-based humidity sensor can be considered as an ideal capacitor **[**33**]**, according to the theory of dielectric physics. The capacitance of an ideal capacitor is independent of the frequency [34].

As the relative humidity increases, more and more water molecules are adsorbed and leakage conduction appears [35]. The capacitance (C) of the leakage-conducting material can be expressed using the following expression (Eq. 1) [36]:

$$C = \varepsilon^* C_0 = \left(\varepsilon_r - i\frac{\gamma}{\omega \varepsilon_0}\right) C_0 \qquad (1)$$

where $\mathcal{E}$* is the complex dielectric parameter, C_0 and $\mathcal{E}_r$ are the capacitance and relative dielectric parameter of an ideal capacitor, respectively. $\mathcal{E}_0$ is the permittivity in a vacuum, γ is leak conductance, and ω is the angular frequency.

This equation shows that the capacitance of the sensing material is inversely proportional to frequency ω and proportional to γ. Therefore, the capacitance value (C) decreases when the frequency increases and this decrease becomes more noticeable as the relative humidity increases (RH = 90 %).

Fig. 7 shows the effect of relative humidity on impedance at different frequencies. It can be seen that the impedance of the NBT-06BT humidity sensor is influenced by the frequency. At low frequencies, the impedance of the NBT-06BT humidity sensor decreases considerably with increasing humidity. In the range of 15 % to 90 % RH, the impedance decreased from 9.1 × 10^3 kΩ to 9.26 kΩ, covering three orders of magnitude at 100 Hz.

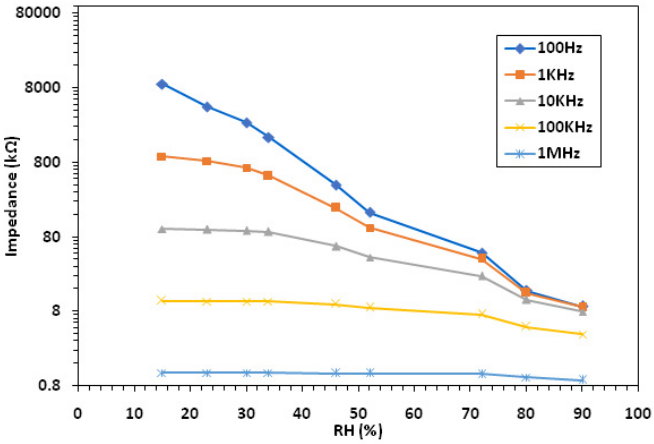

Fig. 7. Impedance versus RH curves for NBT-06BT humidity sensor at various frequencies.

At high frequencies, the impedance curves become flat, indicating that the impedance of the NBT-06BT humidity sensor becomes independent of humidity. The flat impedance curve can be attributed to the dielectric phenomenon [37]. At high frequencies, the adsorbed water molecules are difficult to polarize, which leads to a very small decrease in impedance [14]. The sensitivity of the humidity sensor NBT-06BT has been calculated using equation (Eq. 2) [38]:

$$S = \frac{Z_0 - Z_{\Delta Z\%}}{Z_{\Delta Z\%}} * 100 \qquad (2)$$

where S is sensitivity, Z_0 and $Z_{\Delta Z\%}$ are the impedance of the sensor at 15 % RH and after the change in RH respectively.

The sensitivity of the NBT-06BT humidity sensor at different frequencies is shown in Fig. 8. It can be seen that the sensitivity of the NBT-06BT sensor increases considerably with increasing relative humidity, with a high sensitivity being observed at 100 Hz. According to

the results of Figs 7 and 8, the operating frequency of 100 Hz is used in the remainder of this study.

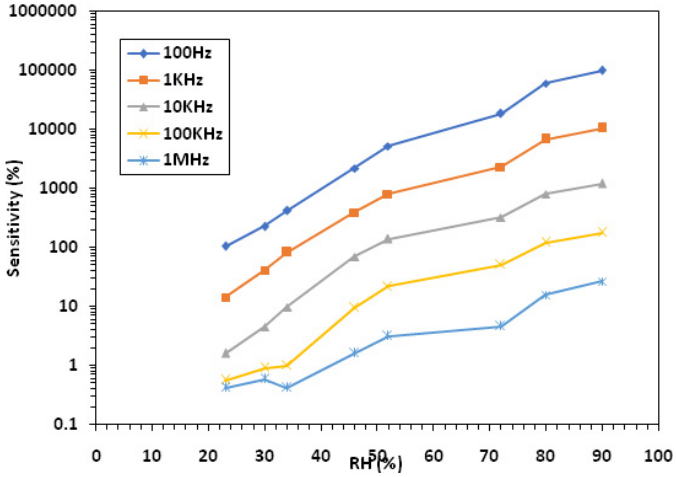

Fig. 8. Sensitivity versus RH curves for NBT-06BT humidity sensor at different frequencies.

Response and recovery time measurements were performed by recording the impedance of the NBT-06BT sensor when relative humidity varies between 15 % and 72 % (with a voltage frequency f = 100 Hz). Fig. 9 shows the response and recovery properties of the NBT-06BT humidity sensor when the humidity changes from 15% RH to 72 % RH and then returns to 15% RH. According to the literature [19**]**, the response and recovery times are defined as the time taken to reach 90 % of the total impedance change. For theNBT-06BT humidity sensor, the response time (when the air humidity varies from 15 % to 72 % RH) is about 68 s and the recovery time (when the air humidity varies from72 % to 15 % RH) is about 125 s. The recovery time is much longer than the response time, indicating that the rate of water desorption is slower than that of adsorption [39]. The processes of water vapor adsorption and desorption correspond to the exothermic and endothermic processes respectively; the endothermic process speed is slower than the exothermic process [40].

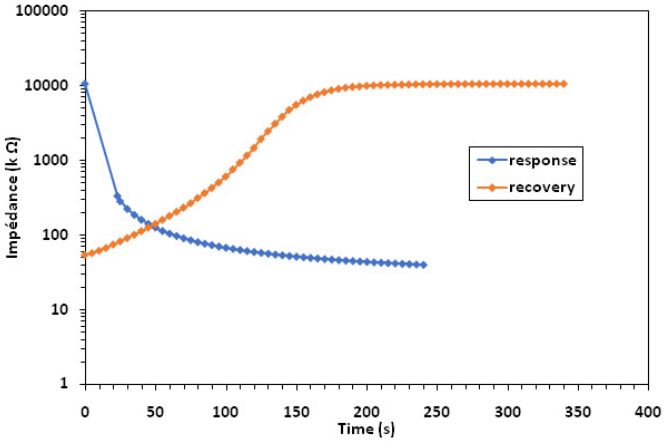

Fig. 9. Response and recovery time of NBT-06BT humidity sensor at 100 Hz.

Humidity hysteresis is an important characteristic used to determine the stability and reliability of a humidity sensor. In our experiment, the hysteresis property is tested by

increasing the humidity from 15 % to 90 % RH (adsorption mode) and then decreasing it from 90% to 15% RH (desorption mode) at the operating frequency of 100 Hz. The humidity hysteresis characteristic at 100 Hz of the NBT-06BT humidity sensor is shown in Fig. 10, with the blue line representing the adsorption process and the red line representing the desorption process. It can be seen that the NBT-06BT humidity sensor has a narrow hysteresis loop during the cyclic variation of the humidity; the impedance measured during the desorption process is slightly lower than that of the adsorption process.

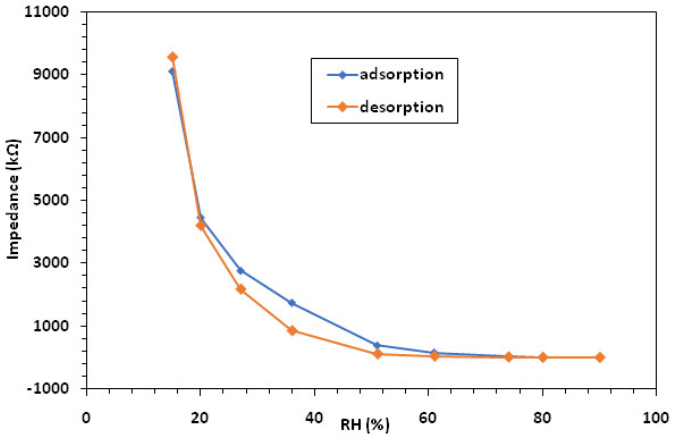

Fig. 10. Humidity hysteresis characteristics of NBT-06BT humidity sensor at 100 Hz.

The formation of the hysteresis loop is caused by the fact that desorption is slower than adsorption and these results are consistent with the results obtained from the curve showing response and recovery **(**Fig. 9**)** [39]. The humidity hysteresis error (γH) was calculated using the expression (Eq. 3) [41]:

$$\gamma H = \pm \frac{\Delta H_{max}}{2F_{FS}} \qquad (3)$$

where ΔH_{max} is the maximum hysteresis value and F_{FS} is the full-scale output.

The NBT-06BT humidity sensor has a maximum hysteresis of about 4.69 % RH during cyclic variation of the relative humidity, indicating good sensor reliability. This shows that even if there is a hysteresis between adsorption and desorption, and thus between response and recovery time, these differences are not important.

3.3. Humidity sensing mechanism

Complex impedance curves are used to analyze the humidity sensing mechanism [42]. Fig. 11 shows the complex impedance spectra of the NBT-06BT humidity sensor, which are measured at a frequency ranging from 100 Hz to 1 MHz with relative humidity ranging from 15 % to 90 %. ReZ and ImZ are the real and imaginary parts of the complex impedance. In Fig. 11(a), at 15 % relative humidity, the impedance spectrum of the NBT-06BT humidity sensor shows a nearly straight line and the impedance value is extremely high. In cases of low relative humidity (23 %, 30 % and 34 %), it can be noticed that the impedance value is still high and the impedance spectra have an arc shape. In Fig. 11(b), with the high relative humidity values (46 %, 52 %, 72 %, 80 % and 90 %), it can be seen that the arc of the impedance spectra gradually becomes a semicircle and the impedance value decreases sharply.

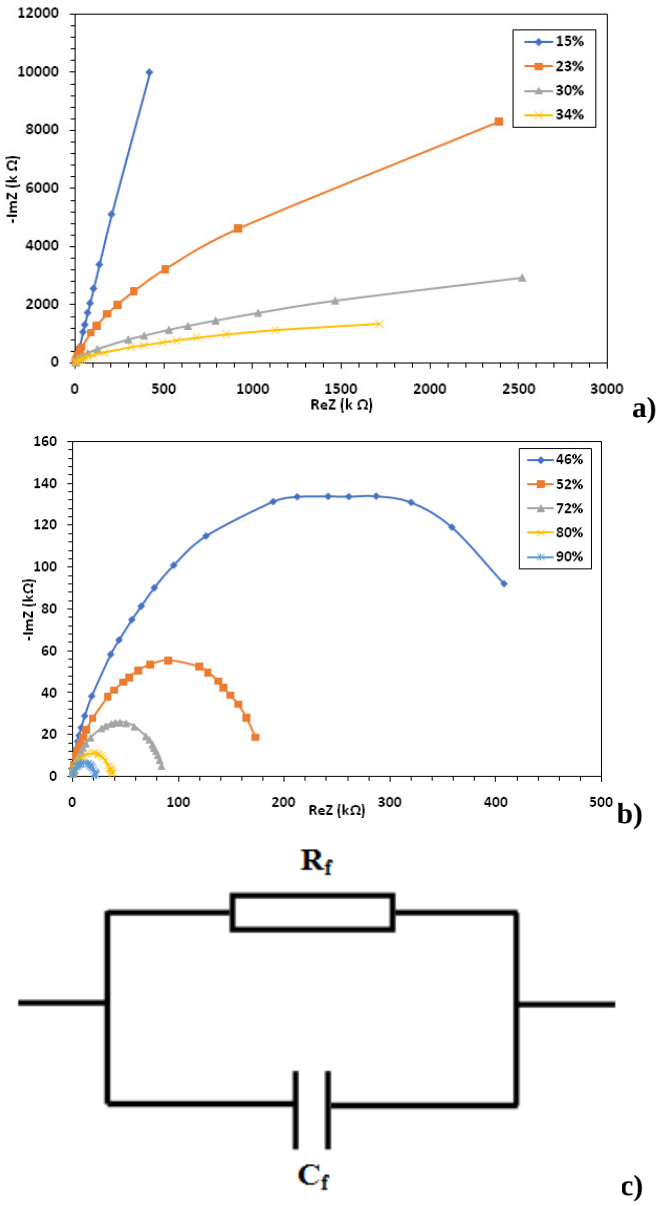

Fig. 11. Complex impedance plots of NBT-06BT humidity sensor at (a) 15-34 % RH, (b) 46-95 % RH, and (c) the equivalent circuit of NBT-06BT humidity sensor.

Complex impedance curves make it possible to differentiate between two conduction mechanisms [43, 44]. In the complex impedance curves, the semicircle corresponds to the protonic transport and the straight line corresponds to the electrolytic conduction [7]. The semicircle can be explained by the non-Debye theory [15]. At low humidity conditions, a small amount of water molecules is adsorbed and the coverage of water on the surface is not continuous. Electrolytic conduction is therefore difficult [45]. However, protonic transport is based on the conductivity of a stable hydronium ion (H_3O^+) that releases a proton to a neighboring water molecule which accepts it while releasing another proton, and so forth, the so-called Grotthuss chain reaction ($H_2O + H_3O^+ \rightarrow H_3O^+ + H_2O$) [46]. Meanwhile, the presence of alkali ions could create more surface defects and oxygen vacancies, resulting in an increase in the number of adsorption sites for water molecules **[8]**. This may make the proton hopping faster and easier, and increase the conduction of the material NBT-06BT. The

results obtained indicate that protonic transport is the dominant conduction mechanism at low and high relative humidity for the NBT-06BT sensor.

The NBT-06BT humidity sensor can be modeled by an equivalent electrical circuit of parallel resistor and capacitor as shown in figure 11(c), this electrical circuit explains the semicircular characteristic of the impedance spectra [47]. R_f and C_f represent the resistance and capacitance of the material NBT-06BT, respectively. In this case, the capacitance C_f is small and the impedance change of the humidity sensor is mainly determined by the resistance R_f [48].

As already mentioned, the decrease in impedance of the NBT-06BT humidity sensor with increasing relative humidity can be attributed to the adsorption of water molecules on the surface of the NBT-06BT sensor [43]. The detection mechanism of the NBT-06BT humidity sensor is based on the adsorption of water molecules on the surface of the NBT-06BT material; the adsorption can be divided into two steps: first, chemisorption and then physisorption. Under conditions of low relative humidity, as the water molecules are polar, they begin to chemisorb (Step I: chemisorption) forming hydrogen bonds with the oxygen atoms on the surface of the NBT-06BT electro-ceramic. At low humidity, after the first layer of water molecules is adsorbed on the surface, a dissociation mechanism leads to the formation of a hydroxide ion (OH^-) and a proton (H^+) from each water molecule [49]. The first is chemically adsorbed on the surface metal ions (Na^+) and the second associates with a surface oxygen ion to form a second hydroxide ion [50]. As a result, electrons accumulate on the surface of the NBT-06BT electro-ceramic, leading to a decrease in the impedance of the NBT-06BT material with increasing relative humidity. When the chemisorption process is complete, several successive layers of water molecules are physisorbed (Step II: physisorption) on the chemisorbed layer at high relative humidity. The physisorbed water layers have liquid-like behavior and the H^+ ions move freely. The conduction process occurs mainly through the Grotthuss transport mechanism [51]. The free movement of H^+ ions on the water layer causes a decrease in the impedance of the electro-ceramic NBT-06BT.

4. Conclusion

In summary, a humidity sensor based on the ceramic material NBT-06BT was successfully fabricated. The ceramic material NBT-06BT was synthesized by the semi-solid method. The humidity sensing properties of the NBT-06BT sensor have been thoroughly investigated. The NBT-06BT humidity sensor has high sensitivity and better linearity at an operating frequency of 100 Hz. The impedance decreases by three orders of magnitude with increasing relative humidity from 15 to 90 % at the frequency of 100 Hz. The response time and recovery time are about 68 s and 125 s respectively, and the maximum hysteresis is 4.69 % RH at 100 Hz. These results show that the NBT-06BT sensor has good humidity detection characteristics. The ceramic material NBT-06BT has good prospects for application as a humidity sensor.

5. References

1. A. E. Dessler, S. C. Sherwood, A matter of humidity, Science 323 (2009) 1020-1021.
2. H. Bi, K. Yin, X. Xie, J. Ji, S. Wan, L. Sun, M. Terronses, M.S. Dresselhaus, Ultrahigh humidity sensitivity of graphene oxide, Scientific reports 3 (20132714.
3. X. Wang, B. Ding, J. Yu, M. Wang, F. Pan, A highly sensitive humidity sensor based on a nanofibrous membrane coated quartz crystal microbalance, Nanotechnology 21 (2010) 055502.

4. Y. Zhang, X.J. Zheng, T. Zhang, L.J. Gong, S.H. Dai, Y.Q. Chen, Humidity sensing properties of the sensor based on $Bi_{0.5}K_{0.5}TiO_3$ powder, Sens. Actuators B Chem. 147 (2010) 180-184.
5. U. Mogera, A.A. Sagade, S.J. George, G.U. Kulkarni, Ultrafast response humidity sensor using supramolecular nanofiber and its application in monitoring breath humidity and flow, Scientific reports 4 (2014) 4103.
6. Z. Chen, C. Lu, Humidity sensors: a review of materials and mechanisms, Sens. letters, 3(4) (2005) 274-295.
7. R. Wang, D. Wang, Y. Zhang, X. Zheng, Humidity sensing properties of $Bi_{0.5}(Na_{0.85}K_{0.15})_{0.5}Ti_{0.97}Zr_{0.03}O_3$ microspheres: Effect of A and B sites co-substitution, Sens. Actuators B Chem. 190 (2014) 305-310.
8. Y. Zhang, X. Zheng, T. Zhang, Characterization and humidity sensing properties of $Bi_{0.5}Na_{0.5}TiO_3$–$Bi_{0.5}K_{0.5}TiO_3$ powder synthesized by metal-organic decomposition, Sens. Actuators B Chem.156(2) (2011) 887-892.
9. R. Wang, Y. He, T. Zhang, Z. Wang, X. Zheng, L. Niu, F. Wu, DC and AC analysis of humidity sensitive properties based on K^+ doped nanocrystalline $LaCo_{0.3}Fe_{0.7}O_3$,Sens. Actuators B Chem. 136(2) (2009) 536-540.
10. H. Hammouche, H. Achour, S. Makhlouf, A. Chaouchi, M. Laghrouche, A comparative study of capacitive humidity sensor based on keratin film, keratin/graphene oxide, and keratin/carbon fibers, Sensors and Actuators A: Physical 329 (2021) 112805.
11. Q. Qi, T. Zhang, Q. Yu, R. Wang, Y. Zeng, L. Liu, H. Yang, Properties of humidity sensing ZnO nanorods-base sensor fabricated by screen-printing, Sens. Actuators B Chem. 133(2) (2008) 638-643.
12. X. Q. Fu, C. Wang, H. C. Yu, Y. G. Wang, T. H. Wang, Fast humidity sensors based on CeO_2 nanowires, Nanotechnology, 18(14) (2007) 145503.
13. J. Wang, Q. Lin, R. Zhou, B. Xu, Humidity sensors based on composite material of nano-$BaTiO_3$ and polymer RMX, Sens. Actuators B Chem. 81(2-3) (2002) 248-253.
14. P. M. Faia, C. S. Furtado, A. J. Ferreira, Humidity sensing properties of a thick-film titania prepared by a slow spinning process,Sens. Actuators B Chem. 101(1-2) (2004) 183-190.
15. K. Khalfaoui, K. Boumchedda, A. Chaouchi, M. Saidi, N. Lamrani, R. Djafar, Impedance Spectroscopy Studies on Steatite with B_2O_3 Ceramics Materials from Algerian Palygorskite, Science of Sintering, 53 (2021) 519-534.
16. Z. Li, H. Zhang, W. Zheng, W. Wang, H. Huang, C. Wang, A. G. MacDiarmid, Y. Wei, , Highly sensitive and stable humidity nanosensors based on LiCl doped TiO_2 electrospun nanofibers,J. Am. Chem. Soc. 130(15) (2008) 5036-5037.
17. Q. Kuang, C. Lao, Z. L. Wang, Z. Xie, L. Zheng, High-sensitivity humidity sensor based on a single SnO_2 nanowire, J. Am. Chem. Soc. 129(19) (2007) 6070-6071.
18. J. Živojinović, D. Kosanović, V. A. Blagojević, V. P. Pavlović, N. Tadić, B. Vlahović, V. B. Pavlović, Dielectric Properties of Mechanically Activated Strontium, Titanate Ceramics, Science of Sintering, 54 (2022) 401-414.
19. Y. He, T. Zhang, W. Zheng, R. Wang, X. Liu, Y. Xia, J. Zhao, Humidity sensing properties of $BaTiO_3$ nanofiber prepared via electrospinning, Sens. Actuators B Chem. 146(1) (2010) 98-102.
20. L. Jingbo, L. Wenchao, Z. Yanxi, W. Zhimin, Preparation and characterization of Li^+-modified $Ca_xPb_{1-x}TiO_3$ film for humidity sensor, Sens. Actuators B Chem. 75(1-2) (2001)11-17.
21. Y. H. Jeong, S. H. Lee, J. H.Yoo, C. Y. Park, Voltage gain characteristics of piezoelectric transformer using $PbTiO_3$ system ceramics, Sens. Actuators APhys. 77(2) (1999) 126-130.

22. Y. Guo, K. I. Kakimoto, H. Ohsato, Dielectric and piezoelectric properties of lead-free $(Na_{0.5}K_{0.5})NbO_3$–$SrTiO_3$ ceramics, Solid State Commun. 129(5) (2004) 279-284.
23. L. Chen, H. Fan, M. Zhang, C. Yang, X. Chen, Phase structure, microstructure and piezoelectric properties of perovskite $(K_{0.5}Na_{0.5})_{0.95}Li_{0.05}NbO_3$–$Bi_{0.5}(K_{0.15}Na_{0.85})_{0.5}TiO_3$ lead-free ceramics, J. Alloys Compd. 492(1-2) (2010) 313-319.
24. D. Biswas, P. Sharma, N. S. Panwar, Effect of Sintering on the Piezoelectric Properties andMicrostructure of Lead Free $(Ba_{1-x}Ca_xZr_{0.1}Ti_{0.9}O_3)$ (x = 0.065) Ceramics, Science of Sintering, 54 (2022) 201-209.
25. J. W. Fergus, Perovskite oxides for semiconductor-based gas sensors, Sens. Actuators B Chem. 123(2) (2007) 1169-1179.
26. J. Zhao, Y. Liu, X. Li, G. Lu, L. You, X. Liang, F. Liu, T. Zhang, Y. Du, Highly sensitive humidity sensor based on high surface area mesoporous $LaFeO_3$ prepared by a nanocasting route. Sens, Actuators B Chem. 181(2013) 802-809.
27. A. Cavalieri, T. Caronna, I. Natali Sora, J. M. Tulliani, Electrical characterization of room temperature humidity sensors in $La_{0.8}Sr_{0.2}Fe_{1-x}Cu_xO_3$ (x= 0, 0.05, 0.10), Ceram. Int. 38(4) (2012) 2865-2872.
28. M. Rawat, K. L. Yadav, Structural, dielectric and ferroelectric properties of $Ba_{(1-x)}(Bi_{0.5}Na_{0.5})_xTiO_3$ ceramics, Ceram. Int. 39(4) (2013) 3627-3633.
29. Y. Guo, D. Akai, K. Sawada, M. Ishida, Dielectric and ferroelectric properties of highly (100)-oriented $(Na_{0.5}Bi_{0.5})_{0.94}Ba_{0.06}TiO_3$ thin films grown on $LaNiO_3/\gamma$-Al_2O_3/Si substrates by chemical solution deposition, Solid state Sci. 10(7) (2008) 928-933.
30. A. Andrei, N. D. Scarisoreanu, R. Birjega, M. Dinescu, G. Stanciu, F. Craciun, C. Galassi, Pulsed laser deposition of lead-free $(Na_{0.5}Bi_{0.5})_{1-x}Ba_xTiO_3$ ferroelectric thin films with enhanced dielectric properties, Appl. Surf. Sci. 278 (2013) 162-165.
31. M. Yuan, Y. Zhang, X. Zheng, B. Jiang, P. Li, S. Deng, Humidity sensing properties of $K_{0.5}Na_{0.5}NbO_3$ powder synthesized by metal organic decomposition, Sens. Actuators B Chem. 209 (2015) 252-257.
32. L. Singh, U. S. Rai, K. D. Mandal, Dielectric, modulus and impedance spectroscopic studies of nanostructured $CaCu_{2.70}Mg_{0.30}Ti_4O_{12}$ electro-ceramic synthesized by modified sol–gel route, J. Alloys Compd. 555 (2013) 176-183.
33. Q.Wang, Y. Z. Pan, S. S. Huang, S. T. Ren, P. Li, J. J. Li, Resistive and capacitive response of nitrogen-doped TiO_2 nanotubes film humidity sensor, Nanotechnology 22(2) (2010) 025501.
34. T. Zhang, Y. He, R. Wang, W. Geng, L. Wang, L. Niu, X. Li, Analysis of dc and ac properties of humidity sensor based on polypyrrole materials, Sens. Actuators B Chem. 131(2) (2008) 687-691.
35. Z. Wang, L. Shi, F. Wu, S. Yuan, Y. Zhao, M. Zhang, The sol–gel template synthesis of porous TiO_2 for a high-performance humidity sensor, Nanotechnology 22(27) (2011) 275502.
36. P. Li, X. Zheng, Y. Zhang, M. Yuan, B. Jiang, S. Deng, Humidity sensor based on electrospun $(Na_{0.5}Bi_{0.5})_{0.94}TiO_3$–$Ba_{0.06}TiO_3$ nanofibers, Ceram. Inter. 41(10)(2015) 14251-14257.
37. A. Sun, L. Huang, Y. Li, Study on humidity sensing property based on TiO_2 porous film and polystyrene sulfonic sodium. Sens, Actuators B Chem. 139(2) (2009) 543-547.
38. Y. Gu, H. Jiang, Z. Ye, N. Sun, X. Kuang, , W. Liu, X. Tang, Impact of size on humidity sensing property of copper oxide nanoparticles,Electro. Mater. Lett. 16(1)(2020) 61-71.
39. M. S.Gong, M. H. Lee, H. W. Rhee, Humidity sensor using cross-linked copolymers containing viologen moiety, Sens. Actuators B Chem. 73(2-3) (2001) 185-191.
40. D. Saha, R. Giri, K. K. Mistry, K. Sengupta, Magnesium chromate–TiO_2 spinel tape cast thick film as humidity sensor, Sens. Actuators B Chem. 107(1) (2005) 323-331.

41. S. Yu, H. Zhang, C. Chen, C. Lin, Investigation of humidity sensor based on Au modified ZnO nanosheets via hydrothermal method and first principle, Sens. Actuators B Chem. 287(2019) 526-534.
42. Y. Sadaoka, M. Matsuguchi, Y. Sakai, S. Mitsui, Electrical properties of α-zirconium phosphate and its alkali salts in a humid atmosphere. J.Mater.Sci. 23(8) (1988) 2666-2675.
43. B. M. Kulwicki, Humidity sensors, J. Am. Ceram. Soc. 74(4) (1991) 697-708.
44. G. Garcia-Belmonte, V. Kytin, T. Dittrich, J. Bisquert, Effect of humidity on the ac conductivity of nanoporous TiO_2, J. Appl. Phys. 94(8) (2003) 5261-5264.
45. Y. Xue-Jun, H. Tian-Sheng, X. U. Xing, L. Zhen, High-performance humidity sensors based on double-layer ZnO-TiO_2 nanofibers via electrospinning, Chin. Phys. Lett. 28(9) (2011) 090701.
46. E. Traversa, Ceramic sensors for humidity detection: the state-of-the-art and future developments, Sens. Actuators BChem. 23(2-3) (1995) 135-156.
47. G. Gusmano, G. Montesperelli, E. Traversa, G. Mattogno, Microstructure and electrical properties of $MgAl_2O_4$ thin films for humidity sensing, J. Am. Ceram. Soc. 76(3) (1993) 743-750.
48. C. D. Feng, S. L. Sun, H. Wang, C. U. Segre, J. R. Stetter, Humidity sensing properties of Nation and sol-gel derived SiO_2/Nafion composite thin films,Sens. Actuators B Chem. 40(2-3) (1997) 217-222.
49. D. Patil, Y. K. Seo, Y. K. Hwang, J. S. Chang, P. Patil, Humidity sensitive poly (2, 5-dimethoxyaniline)/WO_3 composites, Sens. Actuators BChem. 132(1) (2008) 116-124.
50. W. Qu, J. U. Meyer, A novel thick-film ceramic humidity sensor, Sens. Actuators B Chem. 40(2-3) (1997) 175-182.
51. F. M.Ernsberger, The nonconformist ion, J. Am. Ceram. Soc. 66(11) (1983) 747-750.

Сажетак: *У овој студији испитивана су својства детекције влаге керамике састава* $(Na_{0.5}Bi_{0.5})_{0.94}Ba_{0.06}TiO_3$*, обележеног као NBT-06BT. NBT-06BT керамика је синтетисана получврстом методом и окарактерисана рендгенском дифракцијом и скенирајућом електронском микроскопом. NBT-06BT керамички материјал синтерован на 1100 °C, кристалише у тетрагоналном систему без икакве секундарне фазе и представља хетерогену дистрибуцију зрна полиедарског облика са отвореном интергрануларном порозношћу. Испитивања електричних и диелектричних својстава показују да керамички материјал NBT-06BT показује одличне карактеристике детекције влаге као што су висока осетљивост, добра линеарност и уска хистереза. Импеданса се смањује за три реда величине када се релативна влажност повећа са 15 % на 90 % на 100 Hz. Максимална вредност хистерезе сензора је 4,69 % RH. Време одзива и време опоравка су око 68 секунди, односно 125 секунди. Штавише, механизам детекције и осетљивости је детаљно размотрен анализом комплексних спектара импедансе. Ови резултати указују на потенцијалну примену керамичког материјала NBT-06BT као сензора влаге.*

Кључне речи*: сензори влаге, керамика без олова, својства, комплексне импенданс криве, полу-чврста синтеза.*